

Bond order wave (BOW) phase of the extended Hubbard model: Electronic solitons, paramagnetism, coupling to Peierls and Holstein phonons

Manoranjan Kumar and Zoltán G. Soos

*Department of Chemistry,
Princeton University, Princeton NJ 08544*

(Dated: February 17, 2022)

The bond order wave (BOW) phase of the extended Hubbard model (EHM) in one dimension (1D) is characterized at intermediate correlation $U = 4t$ by exact treatment of N -site systems. Linear coupling to lattice (Peierls) phonons and molecular (Holstein) vibrations are treated in the adiabatic approximation. The molar magnetic susceptibility $\chi_M(T)$ is obtained directly up to $N = 10$. The goal is to find the consequences of a doubly degenerate ground state (gs) and finite magnetic gap E_m in a regular array. Degenerate gs with broken inversion symmetry are constructed for finite N for a range of V near the charge density wave (CDW) boundary at $V \approx 2.18t$ where $E_m \approx 0.5t$ is large. The electronic amplitude $B(V)$ of the BOW in the regular array is shown to mimic a tight-binding band with small effective dimerization δ_{eff} . Electronic spin and charge solitons are elementary excitations of the BOW phase and also resemble topological solitons with small δ_{eff} . Strong infrared intensity of coupled molecular vibrations in dimerized 1D systems is shown to extend to the regular BOW phase, while its temperature dependence is related to spin solitons. The Peierls instability to dimerization has novel aspects for degenerate gs and substantial E_m that suppresses thermal excitations. Finite E_m implies exponentially small $\chi_M(T)$ at low temperature followed by an almost linear increase with T . The EHM with $U = 4t$ is representative of intermediate correlations in quasi-1D systems such as conjugated polymers or organic ion-radical and charge-transfer salts. The vibronic and thermal properties of correlated models with BOW phases are needed to identify possible physical realizations.

PACS numbers: 71.10.Fd, 73.22.Gk, 75.40.Cx, 78.30.-j
Email: soos@princeton.edu

I. INTRODUCTION

Nakamura identified the bond order wave (BOW) phase [1] of the one-dimensional (1D) half-filled extended Hubbard model [2] (EHM, Eq. 1). The key features are broken inversion symmetry, doubly degenerate ground state (gs) and finite magnetic gap E_m in a regular (equally spaced) array. Competition among electron delocalization t , on-site repulsion $U > 0$ and nearest-neighbor repulsion $V > 0$ stabilizes the BOW phase over a narrow range whose boundaries motivated subsequent studies [3–9]. The BOW phase has $V \approx U/2$ and substantial t . The quantum transition to the charge density wave (CDW) phase at large V is first order [4, 5] for $U > U^* \approx 7t$, continuous for $U < U^*$. The BOW/CDW boundary is at $V_c(U)$ for $U < U^*$, while the boundary to the spin-fluid phase with $E_m = 0$ is at $V_s(U) < V_c(U)$. Other half-filled 1D Hubbard models with spin-independent interactions have narrow BOW phases between the spin-fluid and CDW phases [10].

Theoretical studies of the EHM have focused on the quantum phase diagram of an extended array without reference to possible physical realizations. Even for models, however, 1D instabilities and finite temperature must be addressed. The principal goal of this paper is to characterize the BOW phase of the EHM at $U = 4t$, a typical choice for intermediate correlation, with special attention to the consequences of gs degeneracy and finite

E_m . Coupling to Peierls or Holstein phonons requires gs derivatives in the adiabatic (Born-Oppenheimer) approximation, and finite temperature properties are needed to assess physical realizations. It is clearly desirable to understand BOW phases prior to specific applications. Broadly similar properties are expected for other U or other 1D models with spin-independent interactions.

Quasi-1D organic molecular crystals and conjugated polymers have strong electron-phonon (e-ph) coupling and electron-molecular-vibration (e-mv) coupling in addition to intermediate correlation. The Su-Schrieffer-Heeger (SSH) model of polyacetylene has linear e-ph coupling and topological solitons as elementary excitations [11, 12]. The Peierls instability is driven by e-ph coupling and has spectacular e-mv consequences in infrared spectra when inversion symmetry is broken. Conjugated polymers and organic ion-radical salts have been a playground for 1D Hubbard models [12–17] with e-ph and e-mv coupling, variable electron or hole filling, degenerate or nondegenerate gs, and either segregated or mixed stacks. The bandwidth is $4t \approx 10$ eV in polymers and $4t \approx 1$ eV in π -stacks, with comparable intermediate t/U . The Peierls instability of Hubbard-type models is a rich separate topic [18]. We are not aware of work on either e-ph or e-mv coupling in the BOW phase. As shown below, finite E_m and degenerate gs lead to electronic solitons in a rigid regular array that nevertheless resemble SSH solitons. With suitable modification, extensive SSH analysis [12, 14] can be applied to models with a BOW phase.

We recently proposed that a BOW phase is realized in Rb-TCNQ(II), the second polymorph of a tetracyanoquinodimethane salt [19, 20]. The evidence is a 100 K crystal structure ($P\bar{1}$) with regular TCNQ⁻ stacks at inversion centers, negligible spin susceptibility below 140 K that indicates a large E_m , and infrared spectra that demonstrates broken electronic inversion symmetry. Broken C_i symmetry and finite E_m in a regular 1D array are precisely the signatures of a BOW phase [1]. Large E_m indicates proximity to the CDW boundary, and we will so choose V in the EHM at $U = 4t$. We have Rb-TCNQ(II) and alkali-TCNQs in mind, but do not model them explicitly beyond invoking solitons for the temperature dependence of infrared spectra. In addition to values of microscopic parameters, interactions between chains must be addressed in actual models along with the Coulomb interactions and transfer integrals for different stacking motifs. We consider electronic properties of the EHM at $U = 4t$ with linear coupling to Peierls and Holstein phonons. Vibrational degrees of freedom are introduced as needed in the adiabatic approximation.

The EHM describes electronic degrees of freedom in a regular 1D array [2]

$$H_{el} = \sum_{p=1, \sigma}^N -t(a_{p, \sigma}^\dagger a_{p+1, \sigma} + h.c.) + \sum_{p=1}^N (U n_p (n_p - 1)/2 + V n_p n_{p+1}) \quad (1)$$

where $t = 1$ is the unit of energy, h.c. is the hermitian conjugate, $a_{p, \sigma}^\dagger (a_{p, \sigma})$ creates (annihilates) an electron with spin σ at site p , and n_p is the number operator. H conserves total spin. The gs is a singlet ($S = 0$) for $U, V \geq 0$ and even N . The half-filled band with N electrons and N sites has electron-hole (e-h) symmetry $J = \pm 1$ and inversion symmetry C_i at sites that we label as $\sigma = \pm 1$. The correlated many-electron basis increases as $\approx 4^N$ at large N . Valence bond (VB) methods [21, 22] at present yield exact results up to $N = 17$ for low-energy states and the full spectrum up to $N = 10$. Nakamura identified [1] the BOW phase using field theory, symmetry arguments and numerical results up to $N = 12$.

To introduce the EHM phase diagram at 0 K, we define three threshold excitations from the singlet gs: the magnetic gap E_m to the lowest triplet, the gap E_J to the lowest singlet with opposite J , and the gap E_σ to the lowest singlet with opposite C_i . Increasing V at constant U, t drives the system from a spin-fluid phase to a CDW phase. Fig. 1 shows the evolution of E_m, E_J and E_σ with V for $U = 4t, N = 12$. The BOW phase spans $V_s < V < V_c$, where $V_s(N)$ and $V_c(N)$ are defined by the excited-state crossovers $E_\sigma(N) = E_m(N)$ and $E_\sigma(N) = E_J(N)$, respectively. Table I lists the

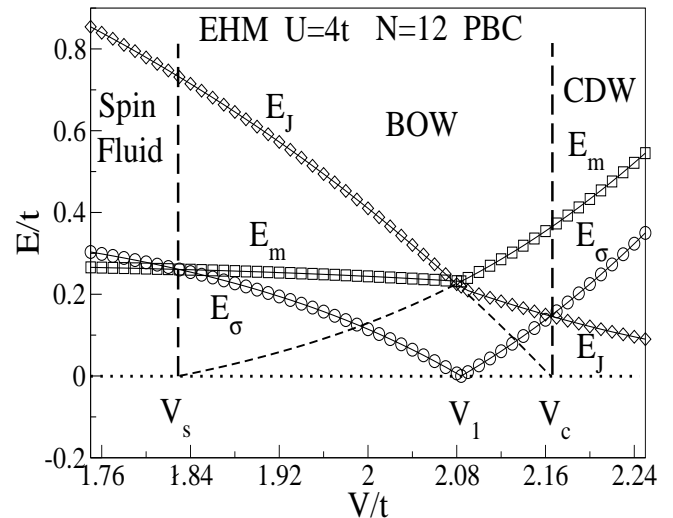


FIG. 1: Excitation thresholds and crossovers of the 12-site extended Hubbard model, Eq. 1, with periodic boundary conditions. E_m, E_σ and E_J are energy gaps to the lowest triplet and the lowest singlets with opposite C_i and e-h symmetry, respectively. V_s is defined by $E_\sigma = E_m$, V_1 by $E_\sigma = 0$ and V_c by $E_\sigma = E_J$.

TABLE I: Excitation thresholds and crossovers of the extended Hubbard model, Eq. 1, with N sites, $U = 4$, and $t_{1N} = \pm 1$ for $N = 4n, 4n + 2$.

N	$V_s (E_\sigma = E_m)$	$V_1 (E_\sigma = 0)$	$V_c (E_\sigma = E_J)$
8	1.8094	2.0597	2.1592
10	1.8190	2.0726	2.1624
12	1.8297	2.0840	2.1645
14	1.8311	2.0925	2.1651
16	1.8452	2.0981	2.1653

remarkably weak size dependence of $V_s(N)$ and $V_c(N)$ for $N = 4n$ with periodic boundary conditions (PBC, $t_{1N} = 1$) and $N = 4n + 2$ with antiperiodic boundary conditions ($t_{1N} = -1$). Similarly, the V_s boundary of a frustrated spin chain has been found [23] using $E_m(N) = E_\sigma(N)$ up to $N = 24$. Multiple methods yield the boundary $V_c(N)$ of the CDW phase [7, 10]. The points $V = V_1(N)$ in Table I or Fig. 1 correspond to $E_\sigma = 0$. They mark a gs degeneracy that is central to our discussion, where broken symmetry gs are readily constructed.

The paper is organized as follows. Broken inversion

symmetry and elementary excitations are treated exactly in Section II for finite N . Electronic solitons, both spin and charge, are found in regular chains with open boundary conditions (OBC, $t_{1N} = 0$) and compared to SSH solitons. Section III deals with linear coupling to molecular (Holstein) and lattice (Peierls) vibrations. The Berry phase formulation of polarization is applied to the infrared activity of molecular vibrations when C_i symmetry is broken. The Peierls instability of the BOW phase is contrasted to the SSH model within the limitations of an adiabatic approximation. The magnetic gap E_m and spin susceptibility χ_M of the BOW phase are obtained in Section IV for large E_m close to the CDW instability. Large E_m reduces the thermal population of excited states and opens a new regime in which spin solitons govern χ_M . The discussion in Section V summarizes the consequences of broken symmetry and finite E_m such as the temperature dependence of the infrared intensity or of χ_M . We briefly mention extensions to BOW phases of related models.

II. BROKEN SYMMETRY AND ELEMENTARY EXCITATIONS

We discuss the EHM, Eq. 1 with $U = 4$, $t = 1$, using exact results for finite N with PBC($t_{1N} = 1$) for $N = 4n$ and $t_{1N} = -1$ for $N = 4n + 2$. The gs kinetic energy is given by the bond orders p_n of successive sites

$$2p_n = \langle \psi_0 | \sum_{\sigma} (a_{n,\sigma}^{\dagger} a_{n+1,\sigma} + h.c.) | \psi_0 \rangle. \quad (2)$$

Broken C_i symmetry in the BOW phase leads to $p_{2n} \neq p_{2n-1}$, while broken e-h symmetry in the CDW phase leads to different electron count $n_{2p} \neq n_{2p-1}$ in the even and odd sublattice. At constant U and t , the order parameter $B(V)$ of the BOW phase is

$$B(V) = |p_{2n}(V) - p_{2n-1}(V)|. \quad (3)$$

$B(V)$ is large between sites $2n$, $2n - 1$ in one broken-symmetry gs and between $2n$, $2n + 1$ in the other.

Since both E_m and E_{σ} vanish rigorously in the spin-fluid phase with $V < V_s$, finite gaps in Fig. 1 are due to finite N . The dashed line $E_m(V) - E_{\sigma}(V)$ is an approximation for opening the magnetic gap. Similarly, the dashed line $E_J(V) - E_{\sigma}(V)$ approximates the closing of the e-h gap at V_c . Finite N limits $E_{\sigma} = 0$ to points $V_1(N)$ in Fig. 1 and Table I. At gs crossovers, we construct broken-symmetry states

$$|\psi_{\pm}(V_1)\rangle = (|\psi_{\sigma=1}\rangle \pm |\psi_{\sigma=-1}\rangle) / \sqrt{2} \quad (4)$$

and compute their bond orders in Eq. 2. Degenerate gs at finite N provide direct access to BOW systems

that is not available for Monte Carlo, which yields the gs energy, or density matrix renormalization group (DMRG) calculations. DMRG with OBC breaks C_i symmetry for even N and returns a nondegenerate gs. We are not aware of DMRG with PBC that conserves C_i and gives the energy and gs in both the $\sigma = \pm 1$ sectors. It is easier to find an energy crossover at $V_1(N)$ where $E_{\sigma} = 0$ for finite N than to demonstrate a degenerate gs over the interval $V_s < V < V_c$ in the extended system.

On the other hand, we need the gs degeneracy at $U = 4t$ beyond the single point $V_1(N)$. To do so, we add the following perturbation to Eq. 1

$$H(J_2) = J_2 \sum_p \vec{S}_p \cdot \vec{S}_{p+2}. \quad (5)$$

$H(J_2)$ acts on second neighbors with one electron each. The upper panel of Fig. 2 shows how $V_1(J_2)$ scans $E_{\sigma} = 0$ across the BOW phase at $U = 4t$, lowering V_1 for antiferromagnetic $J_2 > 0$ and raising it for $J_2 < 0$. The interval $J_2 = \pm 0.15$ in Fig. 2 is sufficient to enforce $E_{\sigma}(J_2) = 0$ between $V/t = 2.0$ and 2.15 for the EHM with $N = 12$ and $U/t = 4$. Strictly degenerate gs in the $\sigma = \pm 1$ sectors will be essential for electron vibrational coupling in Section III.

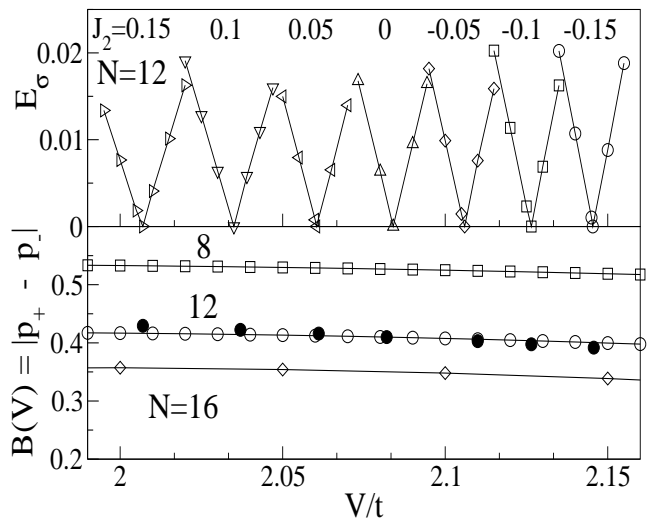


FIG. 2: (top panel) Energy E_{σ} of the lowest singlet with opposite C_i symmetry in a 12-site EHM with $U = 4t$ and PBC as a function of V in Eq. 1 and the indicated J_2 values in Eq. 5. (bottom panel) Order parameter $B(V_1, J_2) = |p_+ - p_-|$ in Eq. 3 at $E_{\sigma} = 0$ for $N = 12$ (closed symbols) and $B(V)$ for $N = 8, 12, 16$ for $J_2 = 0$ (open symbols).

The gs in Eq. 4 and the order parameter B in Eq. 3 hold for $V_1(J_2)$ where $E_\sigma = 0$. The lower panel of Fig. 2 compares $B(V_1(J_2))$ at the indicated J_2 values for $N = 12$ with $B(V)$ based on $J_2 = 0$, when $|\psi_\pm\rangle$ in Eq. 4 are linear combinations of functions that are not quite degenerate. $B(V, N)$ depends weakly on E_σ and N in this interval. Of course, $H(J_2)$ also perturbs other properties, at least slightly, and becomes a strong perturbation for $V < 2t$. We are interested in V close to V_c , where E_σ is small and E_m is large.

Bond orders $p_\pm(V, N)$ and $B(V, N)$ are well approximated near $V \approx V_1(N)$ without invoking J_2 , and results in this Section are based on $J_2 = 0$. For example, $U = 4t$, $V = 2.05t$, $N = 16$ returns $p_+ = 0.752$, $p_- = 0.398$, $B = 0.354$. As expected [24] near the metallic point V_c , the average $p = 0.574$ is within 10% of $2/\pi$, the value for a tight binding (Hückel) band of free electrons with $U = V = 0$ in Eq. 1. The t term dominates near V_c where U and V almost cancel.

The SSH model [11, 12] is a tight-binding band with linear e-ph coupling $\alpha = (dt/du)_0$ to the Peierls phonon, the optical mode of the 1D chain, and an adiabatic approximation for a harmonic lattice. Its gs is dimerized, with $t_n = -(1 - \delta(-1)^n)$ along the stack. Bond orders of the infinite chain are readily found analytically, with $p_+(\delta) = 0.806$, $p_-(\delta) = 0.452$ and $B(\delta) = p_+ - p_- = 0.354$ at $\delta = 0.10$ that matches $B(V)$ of the finite EHM above. The origin of broken C_i symmetry is quite different: e-ph coupling in SSH, correlation U, V in EHM. Moreover, $B(V)$ opens at $V_s \approx 1.86t$ and is almost constant for $V > 2.0t$ before vanishing abruptly at $V_c \approx 2.18t$ while $B(\delta)$ is monotonic in δ . The electronic gs are nevertheless similar and previous discussions of topological solitons or domain walls between regions with opposite B can be applied to BOW phases [12, 14, 15, 26].

We start with electronic domain walls and return later to the Peierls instability. Domain walls are modeled as in SSH with odd N in Eq. 1 and $t_{1N} = 0$. We retain PBC for V to minimize end effects. $N_e = N$ electrons correspond to a neutral soliton with $S = 1/2$, while $N \pm 1$ electrons are charge solitons with $S = 0$. Spin-charge relations are reversed just as in SSH. We label sites from $r = 0$ at the center to $r = \pm(N-1)/2$ at the ends. Positive and negative solitons have equal bond orders by e-h symmetry. We could solve $N = 17$ exactly using a symmetry-adapted valence bond basis to compute p_n in Eq. 2. As shown in Fig. 3 for $N = 15$ and 17, the bond orders of spin and charge solitons are symmetric about the center. They are slightly larger at the chain ends than $p_- = 0.398$, $p_+ = 0.752$, the values of the BOW phase at $V = 2.05t$. This end effect for $t_{1N} = 0$ also appears for even N and alternating bond orders with largest p_+ at either end.

As context for these results, we note that Eq. 1 with

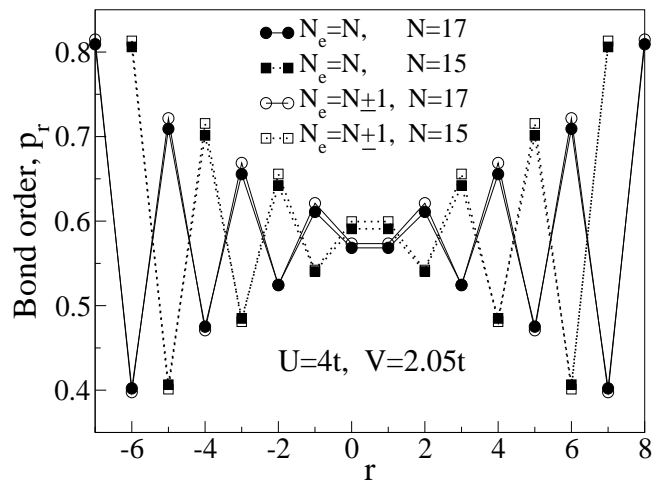


FIG. 3: Bond orders p_r in Eq. 2 of a spin soliton (close symbols) or charge soliton (open symbols) in an N -site EHM with $t_{1N} = 0$, $U = 4t$ and $V = 2.05t$ in Eq.1.

$U = V = 0$ and odd N can be read as a Hückel model of an alternant hydrocarbon with a nonbonding orbital at $\epsilon = 0$ that is empty in the cation, singly occupied in the radical and doubly occupied in the anion. Since the $\epsilon = 0$ orbital has nodes at every other site for any N , it does not contribute to bond orders that are consequently equal for neutral and charge solitons in the SSH model. The correlated model has equal p_r for charge solitons that differ slightly from the spin soliton. In every case, bond orders are p_+ at the ends and reverse smoothly in between.

Next we compute spin densities $\rho_r = 2\langle S_r^z \rangle$ for the radical and charge densities $q_r = 1 - n_r$ for ions. The upper panel of Fig. 4 has ρ_r for $N = 15$ and 17 while the lower panel has q_r for the cation; the anion charges are $-q_r$ by e-h symmetry. The spin or charge density vanishes in alternant hydrocarbons where the nonbonding orbital has nodes, at odd r for $N = 4n + 1$ and even r for $N = 4n - 1$. As seen in Fig. 4, correlation [26] generates small negative ρ_r at these sites and also small q_r of opposite sign. The spin or charge density is large in the middle and decreases at the ends. Electronic solitons in the BOW phase differ in this respect from a regular tight-binding band, which has equal ρ_r or q_r at every other site for any odd N . To mimic the BOW results in Fig. 4 with SSH solitons, finite $\delta \approx 0.05$ is needed for ρ_r and $\delta \approx 0.08$ for q_r since large δ gives faster decrease. Electronic solitons in Figs. 3 and 4 connect regions with $\pm B$ in a regular chain.

Domain walls or topological solitons are the elemen-

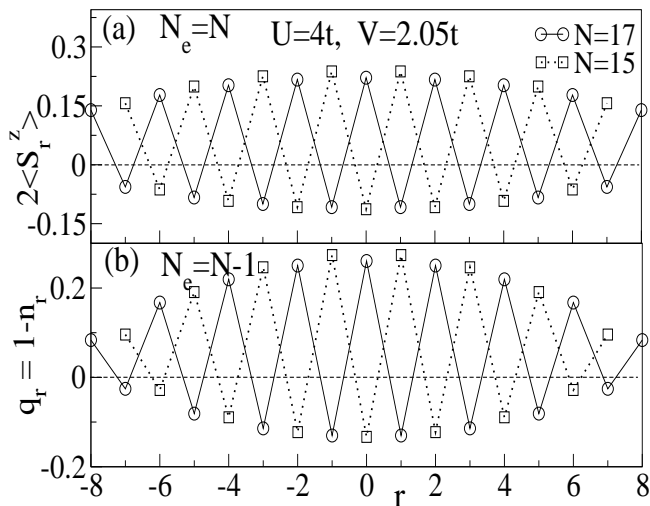


FIG. 4: (a) Soliton spin density $2\langle S_r^z \rangle$ and (b) soliton charge density $q_r = 1 - n_r$ of an N -site EHM with $t_{1N} = 0$, $U = 4t$ and $V = 2.05t$ in Eq. 1.

tary excitations of the BOW phase. They resemble SSH solitons in an appropriately dimerized lattice. The BOW phase has different energy for creating a pair of spin or charge solitons. We take $E_0(N, N_e)$ as the gs energy of Eq. 1 for even N , N_e electrons and $t_{1N} = 0$. The formation energy of a pair of spin solitons ($S = 1/2$) is

$$2W_S(N) = E_0(N+1, N+1) + E_0(N-1, N-1) - 2E_0(N, N). \quad (6)$$

In the limit of large N , parallel spins are the lowest triplet with $2W_S = E_m$, the magnetic gap for PBC. The results for $N = 8, 12$ and 16 in Table II are for $V = V_1(N)$ in Table I, where $E_\sigma = 0$, but the V dependence is weak. The formation energy for a pair of charge solitons is

$$2W_C(N) = E_0(N+1, N) + E_0(N-1, N) - 2E_0(N, N). \quad (7)$$

The cation, anion and neutral system are singlets with different charge. The natural comparison is to the charge gap,

$$2E_C(N) = E_0(N, N+1) + E_0(N, N-1) - 2E_0(N, N). \quad (8)$$

For large N , $E_C(N)$ is the energy of separated ion radicals. As seen in Table II, $2W_C$ approaches E_C from below, as expected since charge solitons are singlets while the ions in E_C are doublets. On the other hand, $2W_C$ is larger than E_J because $V > 0$ favors adjacent

TABLE II: Representative EHM energies in units of t for $U = 4$ and $V = V_1(N)$ in Eq. 1.

Energy, $t = 1$	$N = 16$	$N = 14$	$N = 12$
$2W_S(N)$ Eq.6	0.2116	0.2403	0.2790
$2W_C(N)$ Eq.7	0.9254	1.0281	1.1691
$2E_C(N)$ Eq.8	1.1669	1.2931	1.4610
E_m	0.2124	0.2233	0.2368
E_J	0.3102	0.3046	0.2971
E_3^a	0.8959	1.0094	1.1572

^aThird lowest singlet

sites with $n = 0$ (hole) and $n = 2$ (electron).

Valence bond methods yield low-energy excitations in every symmetry sector with fixed S , J and σ . Except for total wave vector $k = 0$ or π , degeneracy in $\pm k$ is expected and found. Finite-size effects increase with energy and it becomes progressively more difficult to extract more than 3-4 states for large N . The entries in Table II are from a much larger set. An “effective” $\delta_{eff} \approx 0.05 - 0.10$ is inferred from the order parameter $B(V)$ or from spin or charge solitons in the EHM with $U = 4t$ and $2.0 < V/t < V_c$. While BOW-phase results are for a regular stack, they are naturally related to SSH results with $\delta < 0.10$ that is considerably smaller than $\delta = 0.18$ based on the optical gap of polyacetylene[11].

III. COUPLING TO HOLSTEIN AND PEIERLS PHONONS

The SSH model invokes linear e-ph coupling, $\alpha = (dt/du)_0$, to characterize the Peierls instability and elementary excitations of a half-filled tight-binding band. Linear coupling to molecular vibrations is the basis for interpreting polarized infrared spectra of π -radical stacks. The operators $a_{p\sigma}^\dagger$, $a_{p,\sigma}$ create, annihilate electrons with spin σ in the lowest unoccupied molecular orbital of TCNQ, with equal energy $\Delta = 0$ and $n_p = 1$ for a TCNQ⁻ stack. Charge fluctuations [27] modulate Δ and illustrate linear Holstein coupling g_n to the n^{th} totally symmetric (ts) molecular vibration. When C_i symmetry is broken, ts modes become strongly IR allowed by borrowing intensity from the optical charge-transfer excitation and they are polarized along the chain. Accordingly, the appearance of ts modes in polarized IR yields detailed information [28–30] about e-mv coupling constants g_n and has been widely used to infer dimerization. Charge fluctuations break e-h symmetry, and strict degeneracy at $V_1(N)$ is critical because Δ modulation is a small energy.

The Berry-phase formulation [31, 32] of polarization makes possible improved vibronic analysis of extended systems. It is directly applicable to quantum cell models [33] such as the EHM. The polarization P per unit charge

and unit length is a phase [32, 33]

$$P_N = \frac{2\pi}{N} \text{Im}(\ln Z_N) \quad (9)$$

$$Z_N = \langle \psi_0 | \exp(2\pi i M/N) | \psi_0 \rangle \quad (10)$$

$$M = \sum_{p=1}^N p(n_p - 1) \quad (11)$$

where $|\psi_0\rangle$ is the exact gs of an N -site supercell and M is the conventional dipole operator for a regular array with unit spacing. $|Z_N| = 0$ is a metallic point at which P is not defined [31]; it corresponds to V_c for $U < U^*$ and a continuous CDW transition [10]. The EHM has real Z and $P = 0$ by either C_i or e-h symmetry.

The required generalization of Eq. 1 for Holstein coupling in the adiabatic approximation for molecular sites is [33]

$$H(\Delta) = H_{el} + \Delta \sum_{p=1}^N (-1)^p n_p. \quad (12)$$

Finite Δ breaks e-h symmetry, but not C_i symmetry. The gs in the BOW phase is now $|\psi_{\pm}(V, \Delta)\rangle$ with J_2 in Eq. 5 chosen to have $E_{\sigma} = 0$ for $\Delta = 0$. Strictly degenerate $\sigma = \pm 1$ ensures first-order correction in Δ . Finite Δ mixes in excited states such as E_J in Fig. 1 whose energy in the BOW phase decreases rapidly with increasing V . We again vary V at $U = 4$, $t = 1$. Aside from a multiplicative constant, the IR intensity goes as [34]

$$I_{IR}(V) = \left(\frac{\partial P(V, \Delta)}{\partial \Delta} \right)_0^2. \quad (13)$$

Charge fluctuations give a finite derivative at $\Delta = 0$. The IR intensity in Eq. 13 is purely electronic. It can be partitioned among its modes as discussed [28–30] in systems where dimerization breaks C_i symmetry.

We compute the derivative in Eq. 13 in the BOW phase at $V = V_1(J_2)$. The imaginary part of Z_N is initially proportional to Δ , as shown in the inset of Fig. 5. $I_{IR}(V)$ increases rapidly with V up to V_c , as expected for decreasing E_J , and vanishes abruptly in the CDW phase where C_i symmetry is restored and e-h symmetry is broken. The corresponding band result [33, 34] for $(\partial P(\delta, \Delta)/\partial \Delta)_0^2$ increases as $1/\delta^2$ and diverges at the metallic point $\Delta = \delta = 0$ where, however, P is not defined. Since the real part of $Z_N(V) = 0$ at $V = V_c(N)$, the finite system also has divergent $(\partial P(V, \Delta)/\partial \Delta)_0$ at $V_c(N)$ and the BOW phase again resembles a band with small δ , with two major differences. First, $I_{IR}(V)$

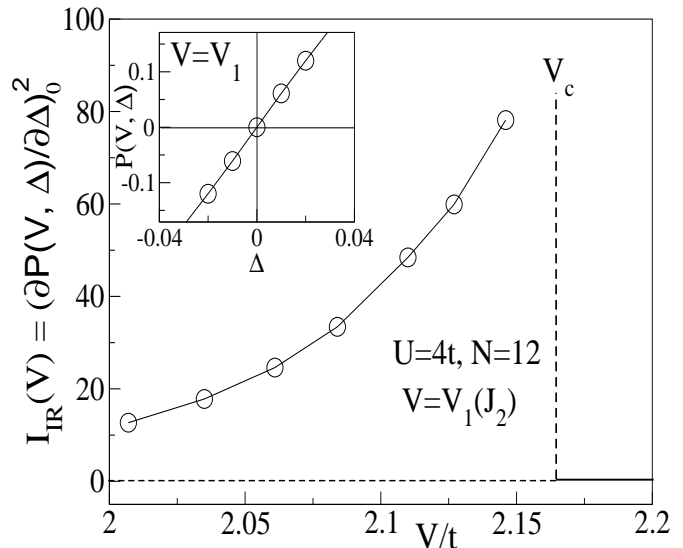


FIG. 5: Infrared intensity $I_{IR}(V)$, Eq. 13, of molecular vibrations due to Δ in Eq. 12 and broken electronic symmetry in the BOW phase of the EHM. The inset is the polarization $P(\Delta)$ in Eq. 9. I_{IR} vanishes by symmetry for $V > V_c$ or $< V_s$.

increases with V up to V_c while $B(V)$ is almost constant. Second, δ_{eff} for IR intensity *decreases* with increasing V up to V_c while δ_{eff} for $B(V)$ *increases* with V from V_s . The SSH model has a single band gap of $4\delta t$ instead of the EHM's multiple threshold excitations in Table I and Fig. 1. For example, the metallic point V_c has large $E_m \approx 0.5t$.

Domain walls introduce inversion centers that reduce I_{IR} between regions with opposite B . More quantitatively, we again consider systems with odd N , $V = 2.05$ and $t_{1N} = 0$. We break C_i symmetry with $\pm\Delta$ at sites $\pm r$ from the center and evaluate $(\partial P/\partial \Delta_r)_0$. Since Δ in Eq. 12 applies all sites in Fig. 5, we scale $P(V, \Delta_r)$ by $N/2$ for the soliton. The inset to Fig. 6 shows $P(V, \Delta_r)$ at $V = 2.05t$ for $\Delta_r = 0.05$, with $P = 0$ at $r = 0$ and scaled $P \approx 0.06$ at the ends of a spin soliton. The same pattern is found for charge solitons (data not shown) with about 50% higher intensity. In either case, $I_{IR}(V)$ at the ends is an order of magnitude less than the $V_1(J_2)$ values for degenerate gs in Fig. 5. This finite-size effect can be traced to higher E_J in the radical. We did not solve $N = 17$ since finite Δ doubles the dimensions of the many-electron basis. IR intensities are consistent with a soliton and an inversion center between regions with $\pm B(V)$.

We consider next the Peierls instability. The SSH

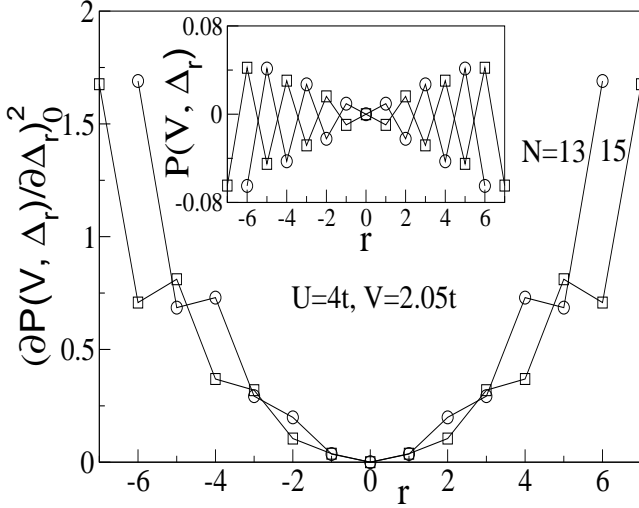


FIG. 6: Infrared intensity $I_{IR}(V)$, Eq. 13, of molecular vibrations due to Δ in Eq. 12 in 13 and 15-site spin solitons with $V = 2.05t$ and $t_{1N} = 0$ in Eq. 1. The inset shows $P(V, \Delta_r)$ for $\Delta_r = 0.30$ in Eq. 9 at site r , with $r = 0$ at the center and $r = \pm(N-1)/2$ at the ends.

model is the generic case for e-ph coupling $\alpha = (dt/du)_0$ in a harmonic 1D lattice with force constant k . Linear coupling is retained in generalizations [18] that require numerical methods and include electron correlation, quantum fluctuations, nonadiabatic or 3D effects, spin chains and models with site energies. Quantum fluctuations are particularly important for small δ that is easily reversed locally. Fluctuations reduce but do not wash out $\delta \approx 0.18$ in the SSH model of polyacetylene [35].

Now Eq. 1 reads

$$H(\delta) = H_{el} + \sum_{p=1, \sigma}^N \delta_p t (a_{p, \sigma}^\dagger a_{p+1, \sigma} + h.c.) + \sum_p \delta_p^2 / 2\epsilon_d. \quad (14)$$

with $\epsilon_d = \alpha^2/k$ and constant $\delta_p = (-1)^p \alpha u/k$ in the gs. The distribution δ_p is subject to the constraint $\sum_p \delta_p = 0$ for a fixed chain length. The gs energy per site is

$$\epsilon_T(\delta) = \epsilon_0(\delta) + \delta^2 / 2\epsilon_d. \quad (15)$$

A minimum at $\delta \neq 0$ implies a dimerized gs. A *global* adiabatic approximation has $\delta(T) > 0$ for $T < T_P$, the Peierls temperature, while a *local* adiabatic approximation leads to domains walls between regions of opposite

δ for $T > 0$.

Our discussion is limited to $\epsilon_T(\delta)$ in Eq. 15. The gs of correlated models is unconditionally dimerized when the regular array has $E_m = 0$ and $\chi_d(\delta) = -(\partial^2 \epsilon_0 / \partial \delta^2)$ diverges at $\delta = 0$. Examples [27] include the ionic phase of organic charge transfer salts and the spin fluid phase of Hubbard models or Heisenberg spin chains. Dimerization is *conditional* at $\epsilon_d \chi_d(0) = 1$ when $\chi_d(0)$ is finite in the neutral phase of CT salts or the CDW phase of the EHM.

Degenerate gs is different, as seen for $N\epsilon_T(\delta)$ in Fig. 7 for $V = V_1(N)$ in Table I and inverse stiffness $\epsilon_d = 0.12$. Now $\epsilon_0(\delta)$ goes as $-B|\delta| - \chi_d(0)\delta^2/2$. The cusp $B(V)$ is due to degeneracy at $\delta = 0$ while the energy gap E_3 in the singlet sector, listed in Table II, ensures finite $\chi_d(0)$. Minimization of ϵ_T yields

$$\delta_{eq} = \pm \epsilon_d B(V) / (1 - \epsilon_d \chi_d(0)) \quad (16)$$

with $\delta_{eq} > 0$ for $\delta > 0$ and $\delta_{eq} < 0$ for $\delta < 0$. Dimerization is unconditional and increases $E_m(\delta)$ beyond $E_m(0)$ as shown in Fig. 7 for a vertical excitation. The gs cusp appears again because the lowest triplet is not degenerate and hence evolves as δ^2 . The slope of $(\partial E_m / \partial \delta)_0$ at the origin is $NB(V_1, N)$. It follows

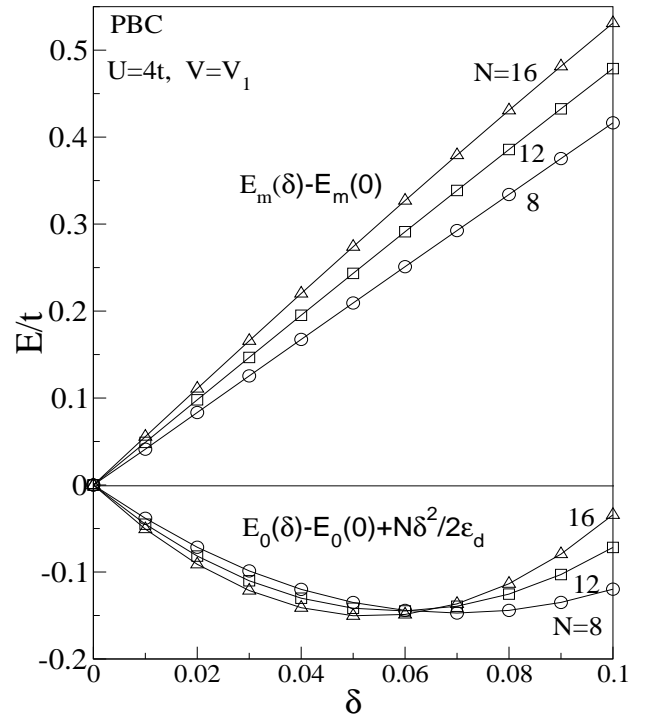


FIG. 7: Ground state energy E_0 in Eq. 15 and magnetic gap E_m of an EHM with dimerization δ in Eq. 14 and $\epsilon_d = 0.12$.

that two domain walls that change the δ_p pattern without changing $\sum_p \delta_p$ lead to lower E_m , and reduced E_m are readily found for $N = 12$ or 16 . Generalization of $2W_S(N)$ in Eq. 6 is more suitable for spin solitons between regions with opposite δ_{eq} . Such simulations are beyond the scope of the present study.

An adiabatic approximation gives a dimerized gs with $\pm\delta_{eq}$ that has to be relaxed locally for solitons. X-ray detection requires that δ_{eq} not be too small compared to the zero point amplitude, $\langle\delta^2\rangle^{1/2}$, of the Peierls phonon $\hbar\omega_P$ in Eq. 15,

$$\langle\delta^2\rangle = \epsilon_d \hbar\omega_P / 2t \quad (17)$$

Typical values [36] of $\hbar\omega_P \approx 100\text{cm}^{-1}$, $\epsilon_d \approx 0.30$ and $t \approx 1500\text{cm}^{-1}$ in organic stacks return $\langle\delta^2\rangle^{1/2} \approx 0.10$ at $T = 0$ that increases with T . Finite E_m and small δ_{eq} minimize contributions from thermal excitations, in contrast to SSH or correlated Peierls systems in which small δ_{eq} necessarily implies small E_m that vanishes at $\delta = 0$. An arbitrarily small perturbation selects one of the degenerate gs of a BOW phase at 0 K, but there is no long-range order in 1D at finite T . Solitons lower the free energy and result in local adiabatic approximations. At low T , the mean separation $R(T)$ between solitons is large compared to their widths 2ξ . Each soliton can then be centered on any of $R(T)$ sites. The soliton density in an extended system with $R > 2\xi$ and $N \rightarrow \infty$ is

$$\rho(T) = \frac{R(T)}{N} = \exp\left(\frac{-W}{k_B T}\right) \quad (18)$$

where k_B is the Boltzmann constant and $W = W_S$ for spin solitons or W_C for charge solitons. The $N = 17$ results in Fig. 4 are not sufficient for estimating 2ξ , but indicate $2\xi > 30$ for spin solitons and $2\xi \approx 30$ for charge solitons, consistent with the SSH estimate [11] of $2\xi \approx 15$ for larger $\delta = 0.18$. Since $W_S < W_C$, spin solitons are thermally accessible and the condition $R(T) > 2\xi$ holds up to $\rho(T) \approx 1\%$.

IV. SPIN SUSCEPTIBILITY

The magnetic gap E_m opens at the boundary V_s of the spin-fluid and BOW phases, and it does so very slowly at a Kosterlitz-Thouless transition [1]. DMRG with PBC provides an independent calculation [10] showing that $E_m(V)$ opens at $V_s = 1.86t$ for the EHM with $U = 4t$. The gap is only $0.023t$ at $V = 2.0$ before reaching $0.241t$ at $V = 2.10$ and $0.63t$ at $V = 2.20$, just in the CDW phase. We are interested in large E_m near the boundary V_c of the BOW and CDW phases in Fig.1. As noted above, V_c is a metallic point with bond orders $p(V)$ in Eq. 2 close to $2/\pi$, the band limit. The band limit returns $E_m = 0$ for

$N = 4n$, when the degenerate orbitals at $\epsilon = 0$ are half filled, and $E_m = 4t\sin(\pi/N)$ for $N = 4n + 2$. Open boundary conditions with $t_{1N} = 0$ have intermediate E_m . The same pattern is seen in Fig. 8 for the EHM at $V = 2.5$, with smallest $E_m(N)$ for $N = 4n$, $t_{1N} = 1$ and $N = 4n + 2$, $t_{1N} = -1$. Quite unusually, E_m increases with N at $V = 2.5$. DMRG calculations [10] of E_m with PBC have minimum $E_m(N)$ at $N \approx 30$ for $V = 2.2$. Exact $E_m(N)$ in Fig. 8 with $t_{1N} = 0$, ± 1 and $V = 2.2$ decrease with N . Rapidly increasing E_m at V_c is also seen [10] for other potentials and has important implications for modeling the spin susceptibility. In particular, larger N is not automatically better.

The molar magnetic susceptibility $\chi_M(T)$ allows quantitative comparisons [13, 25, 37] for organic ion-radical solids with small spin-orbit coupling and g -factors close to the free-electron value, $g = 2.00236$. We take $\chi_M(T)$ to be the spin susceptibility after standard corrections for diamagnetism and impurities. The full spectrum of Eq. 1 is now required, and charge degrees of freedom vastly increase the number of states. We extend exact results for $\chi_M(T)$ up to $N = 10$. The partition function of the EHM in Eq. 1 with even N is

$$Q_N(T) = \sum_{S=0}^{N/2} \sum_{r=1} (2S+1) \exp(-E_{Sr}(N)/k_B T) \quad (19)$$

The singlet gs is the zero of energy, $E_{01}(N) = 0$, and $E_{Sr}(N)$ refers to the state r with spin S . The molar spin susceptibility is

$$\chi_M(T, N) = \frac{N_A g^2 \mu_B^2}{3t N Q_N} \left(\frac{t}{k_B T}\right) \sum_{S=0}^{N/2} \sum_{r=1} S(S+1) \times (2S+1) \exp(-E_{Sr}(N)/k_B T) \quad (20)$$

where μ_B is the Bohr magneton and N_A is Avogadro's number. Finite $E_m = E_{11}$ leads to $\chi_M(0) = 0$, in contrast to finite $\chi_M(0)$ for $V < V_s$ in the spin-fluid phase. We set $E_\sigma = 0$ in the BOW phase and consider finite N to be a coarse-grained approximation of an extended system with a dense spectrum for $E \geq E_m$.

Figure 9 shows $\chi_M(T)$ up to $k_B T = t$ for $N = 8$ with PBC ($t_{1N} = 1$) and $N = 10$ with $t_{1N} = -1$ at $V = 2.10$, 2.15 and 2.20 . Finite-size effects become negligible at high T , as has long been recognized in spin chains. In addition, the broad plateau around $k_B T \approx t$ depends weakly on V , which simply reflects the narrowness of the BOW phase. By contrast, the $T \approx 0$ behavior is governed by $E_m(V)$ and is very sensitive to V at constant U , t . Although $t \approx 10^3\text{K}$ is a small electronic energy, experiment is limited to much lower T . The inset of Fig. 9 expands the relevant range. Finite E_m suppresses χ_M at low T after which χ_M is almost linear in T . The BOW phase of a frustrated spin chain [38] without charge degrees of freedom also has an almost linear $\chi_M(T)$ and

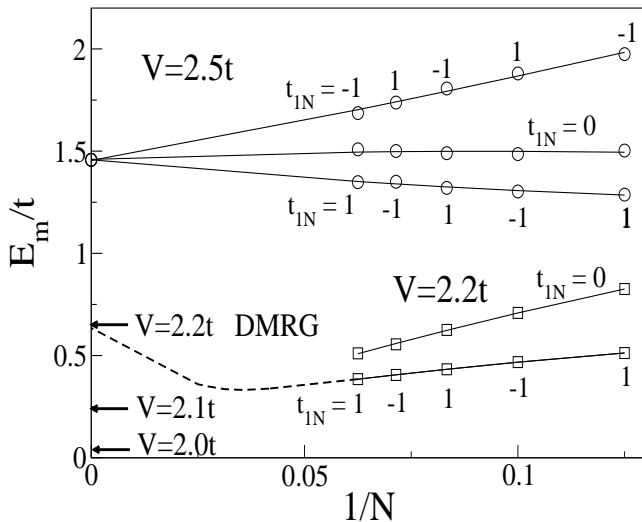


FIG. 8: Magnetic gap E_m of the N -site EHM, Eq. 1, with $U = 4t$ and the indicated V 's. Boundary conditions with $t_{1N} = 0$ and ± 1 are discussed in the text. The DMRG energy gaps are from ref. [10], with minimum E_m around $N \approx 30$ for $V = 2.2t$.

a broad maximum.

A BOW phase with $E_m > 0$ has $\chi_M(T) \approx 0$ up to $T \approx T_1$ followed by a linear increase for $T > T_1$. For example, Rb-TCNQ(II) has [19] $T_1 \approx 140$ K that roughly fixes $t(V)$ in the inset to Fig. 9 and completely specifies $\chi_M(T)$ of the EHM with $U = 4t$. Although $\chi_M(T)$ increases almost linearly to $T = 300$ K, the magnitude at 300 K rules out the $V > 2.10t$ curves in the inset while the $V = 2.10$ curve with $k_B T/t \approx 0.15$ at 300 K fails for T_1 . An EHM with $U = 4t$ is not quantitative for Rb-TCNQ(II). Improved fits are possible for small $\delta_{eq} \approx 0.01$ but such modeling also entails variation of Coulomb interactions.

The EHM boundary V_s between the spin fluid and BOW phases has been difficult to model and has been reported [5] to be as high as $V_s \approx 2.02t$ at $U = 4t$. Since $\chi_M(0)$ is finite in the spin fluid phase and E_m opens slowly for $V > V_s$, very different $\chi_M(T)$ are then calculated in the BOW phase [5]. The evolution of $E_m(V, N)$ in Fig. 8 with N and DMRG results support the original estimate [1] of $V_s \approx 1.86t$ at $U = 4t$ based on excited-state crossovers in Table I. Rapidly increasing $E_m(V)$ as V approaches the metallic point V_c is found in the BOW phase of related Hubbard models [10]. Large E_m is needed for the Rb-TCNQ(II) susceptibility as well as for K and Na-TCNQ at high T where X-ray

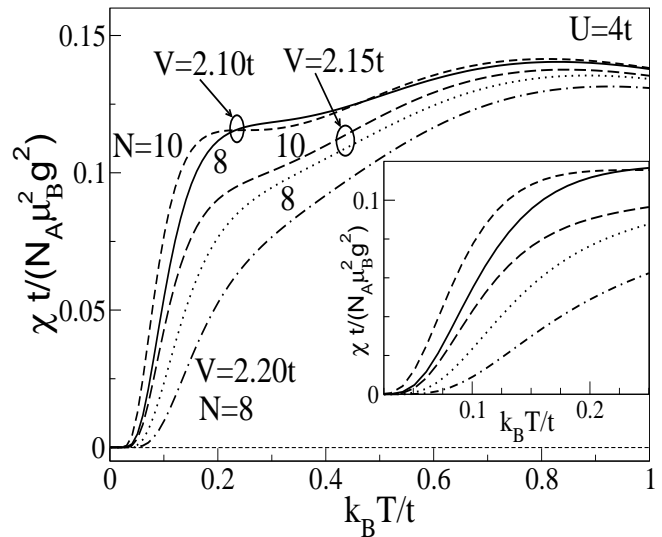


FIG. 9: Temperature dependence of the molar spin susceptibility $\chi_M(T)$ of N -site EHM with $U = 4t$ and V in Eq. 1 The curves in the inset are for the same U, V .

structures [39] indicate regular TCNQ⁻ stacks.

V. DISCUSSION

Rice [28] recognized the possibility of measuring e-mv coupling constants g_n from polarized IR spectra when C_i symmetry is broken on dimerization. Several groups [29, 30] extended the procedure to extracting transferable g_n for selected π -donors and π -acceptors. K-TCNQ was a prime example [40] of a crystal with dimerized TCNQ⁻ stacks at 300 K. Polarized mid-IR spectra show coupled ts modes that are shifted to the red from the corresponding Raman transitions [29, 40]. Powder Rb-TCNQ(II) has virtually identical IR transitions [41] whose polarization along the stack has been confirmed in single crystals [42], but strikingly different temperature dependence. Raman spectra and g_n of TCNQ⁻ are expected to be the same, since solid-state perturbations are usually small [29, 30].

The 100 and 295 K crystal structures of Rb-TCNQ(II) decisively indicate [19] a regular stack of TCNQ⁻ at inversion centers and interplanar separation $R = 3.174 \text{ \AA}$. The 295 K structure is in excellent agreement with previous data [43], and the triclinic space group $P\bar{1}$ is retained at 100K. Low R factors and examination of thermal ellipsoids at 100 K place a conservative limit on dimerization of $R_+ - R_- < 0.05 \text{ \AA}$ [19]. Yet negligibly

small $\chi_M(T)$ below 140 K implies a large E_m and IR data indicates broken electronic C_i symmetry. Broken C_i symmetry in a BOW phase accounts naturally for large E_m near the CDW boundary and for IR intensity at 0 K. We take up the different temperature dependence of the Rb salt.

The IR intensity in Eq. 13 goes as $(\partial P(V, \Delta)/\partial \Delta)_0^2$ [20, 27] and increases with V in the BOW phase as shown in Fig. 5. The intensities for a spin soliton in Fig. 6 are smaller and vanish at the center. Each soliton introduces a C_i center between regions with $\pm B(V)$ and reduces $(\partial P(V, \Delta)/\partial \Delta)_0$ over $\approx 2\xi$ sites. We approximate the temperature dependence as

$$\frac{I_{IR}(T)}{I_{IR}(0)} = \frac{1}{(1 + 2\xi\rho_S(T))}. \quad (21)$$

Here $\rho_S(T)$ is the spin density given by $\chi_M(T)/\chi_C$, where $\chi_C = N_A g^2 \mu_B^2 / 4k_B T$ is the Curie susceptibility. The intensity is 50% lower at $2\xi\rho_S(T) = 1$ where spin solitons overlap. Eq. 21 relates two measured quantities through 2ξ , as shown in Fig. 10 for $2\xi = 60$, which is in the expected range. The $\chi_M(T)$ data is for Rb-TCNQ(II) from ref. [19] and gives $\rho_S(T)$. The intensity ratio of the 722 cm^{-1} mode is from Fig. 2 of ref. [44], with open and closed symbols on cooling and heating. Similar T dependence is seen for other mid-IR modes of crystals [42]. The fit supports a BOW phase interpretation and electronic solitons rather than a specific microscopic model or parameters. A microscopic model must account for $\chi_M(T)$ in addition to the intensity ratio.

We have examined the BOW phase of the EHM at intermediate correlation $U = 4t$ by direct solution of Eq. 1 for finite N . We used degenerate gs at $V = V_1(N)$ in Table I to break inversion symmetry in finite systems and varied J_2 in Eq. 5 to scan $V_1(N)$ over the BOW phase. Exact degeneracy enforced by J_2 turns out to be important for e-ph coupling to Holstein phonons but not for the order parameter $B(V) = p_+ - p_-$ in Eq. 3. We compared BOW properties due to electronic correlation in a regular 1D chain to the SSH model of a dimerized band. SSH results for topological solitons carry over for many aspects of spin and charge solitons in the BOW phase, albeit with different δ_{eff} for different properties. We focused on the consequences of a degenerate gs and finite E_m , especially large E_m close to the metallic point V_c . Broadly similar results are expected in BOW phases of other Hubbard-type models with intermediate correlation.

In the adiabatic approximation for the lattice, linear e-ph coupling generates a dimerized gs in both the BOW phase of the EHM and the SSH model, but they are different. The SSH model has a standard Peierls transition at T_P . Thermal population of excited states stabilizes the regular array for $T > T_P$, and low T_P

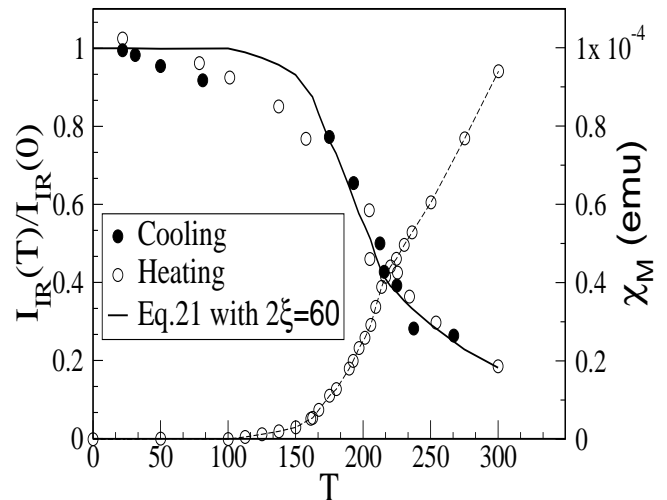


FIG. 10: Intensity ratio $I_{IR}(T)/I_{IR}(0)$ of the 722 cm^{-1} mode of Rb-TCNQ(II) on cooling (open symbols) and heating (closed symbols) from ref [44]. The solid line is Eq. 21 with $2\xi = 60$ and spin density $\rho_S(T)$ from $\chi_M(T)$ in ref. [19]

necessarily implies weak coupling or a stiff lattice. The Peierls transition of polyacetylene is far above its thermal stability, and we are not aware of evidence for $\delta_{eq}(T)$ variations up to ≈ 400 K. Spin-Peierls systems illustrate decreasing $\delta_{eq}(T)$ up to $T_{SP} < 20$ K that can be modeled in the adiabatic approximation [45]. The BOW phase of the EHM at intermediate $U = 4t$ samples a different sector of parameter space, one in which substantial E_m up to $\approx 0.5t$ suppresses thermal excitations. Spin solitons in Eq. 18 with $W_S(\delta)$ give a small $\chi_M(T)$ in this range, and $E_m = 2W_S$ remains finite at $\delta = 0$. The BOW phase has novel aspects that need further study. The principal theoretical issues are quantum fluctuations or nonadiabatic phonons that may suppress a sharp Peierls transition when e-ph coupling is weak. The experimental problem is to detect small dimerization against a background of zero-point motions.

The present discussion is limited to the BOW phase of the EHM at $U = 4t$. We have developed the consequences of coupling to lattice phonons and to molecular vibrations in the adiabatic approximation. Similar results are expected [10] for other quantum cell models with electron-hole symmetry and will be needed to model physical systems with BOW phases, starting with Rb-TCNQ(II). Since alkali-TCNQ salts are semiconductors, they have Coulomb interactions rather than a Hubbard U and are stabilized close to the CDW boundary by the 3D electrostatic (Madelung) energy

[24]. The Na and K-TCNQ salts have dimerization phase transitions [39] with some 3D character since the cations also dimerize. The regular structure at high T has small $\chi_M(T)$ that increases with T in a manner that suggests a BOW phase. Both π -radical organic stacks and conjugated polymers are quasi-1D systems whose initial modeling is without interchain interactions.

In summary, we have characterized the BOW phase of the EHM with intermediate $U = 4t$ by exact treatment of finite systems with degenerate gs at $V = V_1(N)$. The elementary excitations are electronic solitons, both spin and charge, in a regular array. Solitons in the correlated BOW phase resemble the familiar solitons of the SSH model for e-ph coupling in a tight-binding band. Several measures indicate an “effective” dimerization $\delta < 0.10$ that is considerably less than $\delta = 0.18$ for the SSH model of polyacetylene. Charge fluctuations are coupled to molecular (Holstein) phonons that become IR active

in the BOW phase due to broken C_i symmetry. The T dependence of IR modes is consistent with spin solitons whose width is $2\xi \approx 60$ lattice constants. The BOW phase is dimerized at 0 K in the adiabatic approximation, but gs degeneracy and finite E_m lead to novel aspects for a possible Peierls transition. Previous discussions of SSH solitons greatly facilitate analysis of the BOW phase. So have previous treatments of e-ph and e-mv coupling in 1D Hubbard models for conjugated polymers and organic ion-radical or charge-transfer crystals. The BOW phase of Hubbard-type models with intermediate correlation has some unique aspects that invite further study as well as features that are common to such models.

Acknowledgments: ZGS thanks A. Girlando for access to unpublished IR spectra and A. Painelli for discussions of polarization and BOW phases. We thank the National Science Foundation for partial support of this work through the Princeton MRSEC (DMR-0819860).

-
- [1] M. Nakamura, Phys. Rev. B **61**, 16377 (2000); J. Phys. Soc. Jpn. **68**, 3123 (1999).
- [2] J.E. Hirsch, Phys. Rev. Lett. **53**, 2327 (1984); Phys. Rev. B **31**,
- [3] P. Sengupta, A.W. Sandvik and D.K. Campbell, Phys. Rev. B **65**, 155113 (2002).
- [4] Y.Z. Zhang, Phys. Rev. Lett. **92**, 246404 (2004).
- [5] S. Glocke, A. Klumper and J. Sirker, Phys. Rev. B **76**, 155121 (2007).
- [6] S. Ejima and S. Nishimoto, Phys. Rev. Lett. **99**, 216403 (2007).
- [7] G. P. Zhang, Phys. Rev. B **68**, 153101 (2003).
- [8] K-M Tam, S-W Tsai and D.K. Campbell, Phys. Rev. Lett. **96**, 036408 (2006).
- [9] A. Sandvik, L. Barents and D.K. Campbell, Phys. Rev. Lett. **92**, 236401 (2004).
- [10] M. Kumar, S. Ramasesha and Z.G. Soos, Phys. Rev. B **79**, 035102 (2009).
- [11] W.P. Su, J.R. Schrieffer and A.J. Heeger, Phys. Rev. B **22**, 2099 (1980); Phys. Rev. Lett. **44**, 1698 (1979)
- [12] A.J. Heeger, S. Kivelson, J.R. Schrieffer and W.P. Su, Rev. Mod. Phys. **60**, 781 (1988).
- [13] Z.G. Soos, Annu. Rev. Phys. Chem. **25**, 121 (1974); Z.G. Soos and D.J. Klein, in *Treatise on Solid State Chemistry*, Vol. III (ed. N.B. Hannay, Plenum, New York, 1976) p. 689.
- [14] T.J. Skotheim, Ed. *Handbook of Conducting Polymers*, Vol. 2 (Marcel Dekker, New York, 1986).
- [15] D. Jerome, Chem. Rev. **104**, 5565 (2004).
- [16] N.S. Sariciftci (Ed.), *Primary Photoexcitations in Conjugated Polymers: Molecular Exciton Versus Semiconductor Band Model*, World Scientific, Singapore, 1997.
- [17] Z.G. Soos, D. Mukhopadhyay, A. Painelli and A. Girlando, in *Handbook of Conducting Polymers*, Sec. Edit. (Eds. T.A. Skotheim, R. Elsenbaumer and J. R. Reynolds, Marcel Dekker, New York, P997) p. 165.
- [18] P. Sengupta, A.W. Sandvik and D.K. Campbell, Phys. Rev. B **67**, 245103 (2003).
- [19] T.M. McQueen, D.M. Ho, C. Jimenez Cahua, R.J. Cava, R.A. Pascal, Jr., and Z.G. Soos, Chem. Phys. Lett. **475**, **44** (2009).
- [20] Z.G. Soos, M. Kumar, S. Ramasesha and R.A. Pascal, Jr., Physica B **405**, 5353 (2010).
- [21] S. Ramasesha and Z.G. Soos, Int. J. Quant. Chem. **25**, 1003 (1984); Z.G. Soos and S. Ramasesha, Phys. Rev. B **29**, 5410 (1984).
- [22] Z.G. Soos and S. Ramasesha, in *Valence Bond Theory and Chemical Structure*, D.J. Klein and N. Trinajstić, Eds. (Elsevier, Amsterdam, 1989), p. 81; S. Ramasesha and Z.G. Soos, in *Theoretical and Computational Chemistry*, Vol. 10, D.L. Cooper, Ed. (Elsevier, Amsterdam, 2002) p. 635.
- [23] K. Okamoto and K. Namura, Phys. Lett. A **169**, 433 (1992).
- [24] M. Kumar, S. Ramasesha, R.A. Pascal, Jr. and Z.G. Soos, Europhys. Lett. **83**, 37001 (2008).
- [25] S.A. Bewick and Z.G. Soos, Chem. Phys. **325**, 60 (2006); S.A. Bewick and Z.G. Soos, J. Phys. Chem. B **110**, 18748 (2006).
- [26] Z.G. Soos and S. Ramasesha, Phys. Rev. Lett. **51**, 2374 (1983).
- [27] A. Girlando, A. Painelli, S.A. Bewick and Z.G. Soos, Synth. Met. **141**, 129 (2004).
- [28] M.J. Rice, Solid State Commun. **31**, 93 (1979); M.J. Rice, N.O. Lipari and S. Strassler, Phys. Rev. Lett. **21**, 1359 (1977).
- [29] R. Bozio and C. Pecile, in *Spectroscopy of Advanced Materials*, Adv. Spectrosc. Vol. 19, R.J.H. Clark and R.E. Hester, Eds. (Wiley, New York, 1991), p. 1.
- [30] Painelli and A. Girlando, J. Chem. Phys. **84**, 5655 (1986); C. Pecile, A. Painelli and A. Girlando, Mol. Cryst. Liq. Cryst. **171**, **69** (1989).
- [31] R. Resta, J. Phys.: Condens. Matter **14**, R625 (2002).
- [32] R. Resta, Phys. Rev. Lett. **80**, 1800 (1998).
- [33] A. Painelli and Z.G. Soos, Chem. Phys. **325**, 48 (2006); Z.G. Soos, S.A. Bewick, A. Peri and A. Painelli, J. Chem. Phys. **120**, 6712 (2004).
- [34] L. Del Frio, A. Painelli and Z.G. Soos, Phys. Rev. Lett.

- 89**, 27402 (2002).
- [35] W.P. Su, *Solid State Commun.* **42**, 497 (1982).
- [36] M. Masino, A. Girlando and Z.G. Soos, *Chem. Phys. Lett.* **369**, 428-33 (2003); G. D'Avino, A. Girlando, A. Painelli, M-H. Lemee-Cailleau and Z.G. Soos, *Phys. Rev. Lett.* **99**, 156407 (2007).
- [37] J.S. Miller, Ed. *Extended Linear Chain Compounds*, Vol. 3 (Plenum, New York 1983); H.T. Diep, Ed. *Frustrated Spin Systems* (World Scientific, Hackensack, N.J. 2003).
- [38] M. Kumar, S. Ramasesha and Z.G. Soos, *Phys. Rev. B* **81**, 054413 (2010).
- [39] M. Konno and Y. Saito, *Acta Cryst. B* **31**, 2007 (1975); M. Konno, T. Ishii and Y. Saito, *Acta Cryst. B* **33**, 763 (1977).
- [40] D.B. Tanner, C.S. Jacobsen, A.A. Bright and A.J. Heeger, *Phys. Rev. B* **15**, 3283 (1977).
- [41] R. Bozio, I. Zanon, A. Girlando and C. Pecile, *J. Chem. Soc. Faraday Trans.* **274**, 235 (1978).
- [42] A. Girlando, private communication (2008).
- [43] H. Kobayashi, *Bull. Chem. Soc. Jpn.* **54**, 3669 (1981); I. Shirotnani and H. Kobayashi, *Bull. Chem. Soc. Jpn.* **46**, 2595 (1973).
- [44] R. Bozio and C. Pecile, *J. Chem. Phys.* **67**, 3864 (1977).
- [45] Z.G. Soos and S.A. Bewick, *Chem. Phys. Lett.* **421**, 210 (2006); I.S. Jacobs, J.W. Bray, H.R. Hart, L.V. Interrante, J.S. Kasper, G.D. Watkins, D.E. Prober and J.C. Bonner, *Phys. Rev. B* **14**, 3036 (1976).